Newman-Penrose constants and the tails of self-gravitating waves

R. Gómez and J. Winicour

Department of Physics and Astronomy, University of Pittsburgh, Pittsburgh, Pennsylvania 15260

B. G. Schmidt

Max Planck Institute for Astrophysics, D-85740 Garching, Germany

We study the properties of the decay of a self-gravitating radiation field by analyzing the relation between behavior in the weak field regime, test field behavior in a Schwarzschild background, and strong field behavior. Our model consists of a spherically symmetric scalar field incident on a reflecting barrier, which allows all these regimes to be treated on a common nonsingular manifold. Our primary conclusion, in the curved space case, is that there are two distinct types of late decay determined by whether or not the Newman-Penrose constant for the scalar field vanishes. For the nonvanishing case, the radiation tail decays as $1/t$, with respect to Bondi time, but there are also $\ln t/t^2$ corrections, as well as the exponentially decaying contributions associated with quasinormal modes.

I. INTRODUCTION

The theoretical understanding of the decay of the gravitational radiation from a highly general relativistic system will be of great importance in the future of gravitational wave astronomy because it can be used to extract information about the structure of the underlying system from observed waveforms. In the case of black hole formation, it is anticipated that the final decay of the radiation might be quantitatively similar to the ring down of a test wave in a Schwarzschild background. It is expected that the higher order terms in a perturbation expansion be small although there are no theorems in this regard. There is a considerable understanding of the perturbation problem in terms of the quasinormal modes of a Schwarzschild black hole [1]. The quasinormal modes are characterized by exponential time dependence $e^{i\omega t}$ but with complex eigenfrequencies ω which include the effects of radiation damping. However, there is no straightforward mathematical analysis of a system in terms of its quasinormal modes analogous to the normal mode decomposition provided, for example, by Fourier analysis. The role they play in radiative decay has been elucidated in terms of the properties of the Laplace transform of the system [2,3]. The quasinormal eigenfrequencies correspond to the poles of the Green function for the Laplace operator. For the black hole problem, this Green function also has a branch cut which corresponds to a power law decay, in powers of $1/t$, which eventually dominates the exponentially damped quasinormal modes at late time. The ultimate power law decay is expected to be too weak to be observationally important. However, any precise statement of this type is difficult to make and would depend upon the initial conditions of the system in a very sensitive way.

Observing this late time decay by numerical simulation is also a sensitive matter because of the increasingly high redshift between observers at infinity and the central region where gravitational collapse takes place. In the absence of curvature, there is no tail to the outgoing radiation of a spherically symmetric, scalar wave whose initial data have compact support. In previous numerical studies of black hole formation by a self-gravitating spherically symmetric, scalar wave [4], the radiation tail for a compact initial pulse was found to decay exponentially with respect to Bondi time when tracked up to redshift factors of 10^5. The time constant of this exponential decay corresponded closely to the lowest quasinormal mode for scalar perturbations of a Schwarzschild background. However, there was no evidence of power law radiation tails in this redshift regime.

Gundlach, Price, and Pullin [5,6] have recently reexamined the existence of power law tails. By approximations to the perturbation equations for a test field in a Schwarzschild background, they generalized the earlier analysis [1] of power law tails to include the radiation fields at null infinity. Furthermore, they demonstrated the existence of these power law tails in the full nonlinear case by extending numerical simulations to sufficiently high redshifts. The consistency they establish between perturbation theory and numerical evolution of the nonlinear system is very reassuring.

In this paper, we carry out a similar examination, based upon different boundary conditions, different analytic approximations, and different numerical techniques, using the model of a self-gravitating scalar wave. Our work confirms the major results of Gundlach, Price, and Pullin and reveals how the presence or absence of a Newman-Penrose constant differentiates between two different types of power law decay. In addition, we obtain an exhaustive set of analytic solutions at the "linear in m" approximation which reveal a logarithmic correction to the leading order power law decay of the radiation amplitude. Numerical solutions based upon a grid which

compactifies null infinity allows us to accurately distinguish between the different power laws that apply at finite radius and at infinity, as well as to verify that the logarithmic terms appearing in the analytic approximation persist in the nonlinear regime.

Our theoretical model is a spherically symmetric space-time satisfying the coupled Einstein-Klein-Gordon equations for a massless scalar field Φ. We set this as a nonlinear mixed boundary value problem for the region of space-time outside a timelike inner boundary and to the future of an initial null hypersurface. On the inner boundary, we prescribe the intrinsic geometry and extrinsic curvature corresponding to a surface of radius R and mass m in a Schwarzschild space-time and we set the scalar field to zero, so that this boundary acts as a perfectly reflecting barrier. Here m is a free constant subject to the constraint $R > 2m$. The solution then depends solely upon the characteristic data for the scalar field on the initial null hypersurface. This is a well posed $(1+1)$-dimensional boundary value problem. We explore the decay of a scalar wave in (i) the flat space regime, (ii) as a test wave on a Schwarzschild background, and (iii) in the fully general relativistic regime in which it forms its own black hole. The use of a reflecting boundary allows these three regimes to be described smoothly on a common manifold if a judicious choice of coordinate conditions is made (with some technical qualification corresponding to choices of data that might evolve to form weak solutions). We use null-polar coordinates consisting of a retarded time u, which labels the outgoing null cones, and a luminosity distance r, determined by the surface area of the spherical cross sections of these cones. These coordinates also provide a smooth description of future null infinity $\mathcal{J}^+$, in terms of the compactified coordinate $l = 1/r$, in all three regimes.

In this coordinate system, the line element is

$$ds^2 = e^{2\beta} du \left(\frac{V}{r} du + 2dr \right) - r^2 (d\theta^2 + \sin^2\theta d\phi^2), \quad (1.1)$$

and the Einstein-Klein-Gordon equations, for the spherically symmetric case, reduce to [4,7]

$$\beta_{,r} = 2\pi r (\Phi_{,r})^2, \quad (1.2)$$

$$V_{,r} = e^{2\beta}, \quad (1.3)$$

and the scalar wave equation $\Box\Phi = 0$, which takes the form

$$2(r\Phi)_{,ur} = r^{-1}(rV\Phi_{,r})_{,r}. \quad (1.4)$$

The initial null data necessary for evolution consist of $\Phi(u_0, r)$, $r \geq R$, at a given retarded time which we set to be $u_0 = 0$. At the reflecting boundary, $\Phi(u, R) = 0$ and we choose the coordinate condition $\beta(u, R) = 0$, while the boundary conditions imply $V(u, R) = R - 2m$. With these conditions the scalar field and metric components have a unique evolution. The resulting metric does not have an asymptotic Minkowski form in the limit $r \to \infty$ of future null infinity $\mathcal{J}^+$. We set $H(u) = \beta(u, \infty)$. Then Bondi time t at $\mathcal{J}^+$ is related to proper time $\tau = u\sqrt{1 - 2m/R}$ on the reflecting boundary by

$$\frac{dt}{d\tau} = e^{2H} / \sqrt{1 - 2m/R}. \quad (1.5)$$

Bondi time is the physically relevant time for a gravitational wave antenna whereas the internal proper time determines the dynamical time scale of the collapsing wave.

No globally well behaved exact solutions are known for this system. In the next section, the flat space limit is treated analytically and its solution used to generate an analytic solution to first order in m for a test wave in a Schwarzschild background. This solution provides the details of the final decay to this order of approximation. The fully nonlinear, general relativistic case is then treated numerically in Sec. III, using the algorithm for nonlinear scalar waves developed in Refs. [8] and [4]. The numerical solutions display the same critical behavior established for the $m = 0$ case without a reflecting boundary [9]. A weak scalar field is completely radiated to infinity and the world tube of the reflector extends to future time infinity I^+, where the final Bondi mass equals m. However, above a critical strength, the scalar field undergoes gravitational collapse to form a horizon, whose formation is indicated by the redshift factor $dt/d\tau \to \infty$, to within numerical limitations. In this event, some of the scalar field is radiated to infinity and some crosses the horizon. Thus the reflector itself must fall through the horizon, for otherwise it would continue to reflect the scalar field until all its energy were radiated to infinity. Accordingly, the final black hole mass must satisfy $M_H > R/2$, and so, unlike the case without the reflector [10,11], this system exhibits a "mass gap." Critical phenomena for black holes whose mass is close to $R/2$ seem to appear in our model but, as we have not yet made a refined study of this, we focus here on the radiation tail. Agreement with the analytic approximation provides a means of confirming that the numerical description of the tail is valid at the high redshifts marking the transition from exponential decay to power law decay.

II. LINEARIZED WAVES

A. Waves in flat space-time

Setting $m = 0$ and retaining only terms linear in Φ, (1.2) and (1.3) imply $\beta = 0$ and $V = r$ and (1.4) reduces to the flat space wave equation

$$\Box^{(2)} g := 2g_{,ur} - g_{,rr} = 0, \quad (2.1)$$

where $g = r\Phi$. (In this limit, u, t, and τ are all equal.) The general solution satisfying the reflecting boundary condition is

$$g(u, r) = f(u/2 + r) - f(u/2 + R). \quad (2.2)$$

Without loss of generality, we choose $f(r) = g(0, r)$, to satisfy the initial conditions. The first term in (2.2) describes an incoming wave, and the second, its reflection off the boundary.

Smoothness of the scalar field at future null infinity, from the point of view of the Penrose compactification of Minkowski space-time, corresponds to the existence

of an asymptotic Taylor series in powers of $1/r$, i.e., $g = Q + P/r + \cdots$. The leading term $Q(u)$ is the time-dependent monopole moment which carries the radiation energy off to infinity. The next coefficient P has the special property of being time independent. It is an example of a Newman-Penrose constant of the motion [12].

The late time decay of the wave depends upon the initial data. First consider data of compact support, i.e., $g(0, r) = 0$ for $r \geq R_1 \geq R$. Then (2.2) implies that $g(u, r) = 0$ for $u \geq 2(R_1 - R)$. It should be noted that this absence of a tail is peculiar to the spherically symmetric case. In the case of a flat space wave with compact radial support but with $l \neq 0$ spherical harmonic dependence, the reflection off a spherical barrier leads to quasinormal mode decay characterized by a complex eigenfrequency [2].

Next consider noncompact initial data for which g_0 =const for $r > R_1$, i.e., for data corresponding to the static monopole solution $\Phi = Q/r$ in this region. Because of the reflecting boundary, the evolution of these data is not static. However, we again have $f(u/2 + r) - f(u/2 + R) = 0$ for $u \geq 2(R_1 - R)$ so that there is no tail. This is an exceptional case because the evolution of Φ preserves the pure $1/r$ radiation form in the outer region $r \geq R_1$.

Other choices of noncompact data do lead to tails whose decay rate is determined by the far field radial falloff of the data. In particular, consider the family of initial data, parametrized by an integer N, for which

$$g(0, r) = (R/r)^N - 1 \quad \text{for} \quad N > 0, \qquad (2.3)$$

outside the barrier. The solution is

$$g_N(u, r) = \frac{R^N[(u/2 + R)^N - (u/2 + r)^N]}{(u/2 + R)^N(u/2 + r)^N}. \qquad (2.4)$$

The decay rate depends upon the direction of approach. In the limit of time infinity, letting $u \to \infty$ holding r =const, we obtain

$$g_N \sim 2N(2R)^N(R - r)/u^{N+1}. \qquad (2.5)$$

At null infinity, the decay rate of the radiation amplitude $Q(u) = g(u, \infty)$ is obtained by first taking the limit $r \to \infty$ before letting $u \to \infty$. This gives

$$Q_N \sim -(2R/u)^N. \qquad (2.6)$$

The leading term past the monopole Q in the $1/r$ expansion of the initial data $g(0, r)$ determines the decay rate, either according to (2.5) or (2.6). The slowest possible decay rate arises in the case $N = 1$, for which the Newman-Penrose constant is nonzero.

B. Linearized waves in a Schwarzschild space-time

With this background, we now proceed to waves propagating in a Schwarzschild space-time. Retaining only linear terms in Φ, (1.2) and (1.3) now imply $\beta = 0$ and $V = r - 2m$, so that the metric has the (null polar)

Schwarzschild form, and (1.4) reduces to the test wave equation

$$2g_{,ur} - g_{,rr} = -\frac{2m}{r}\left[r\left(\frac{g}{r}\right)_{,r}\right]_{,r}, \qquad (2.7)$$

where again $g = r\Phi$. In terms of the expansion $g = \Sigma g^{(n)} m^n$, this leads to an inhomogeneous flat space wave equation for $g^{(n)}$:

$$2g^{(n)}_{,ur} - g^{(n)}_{,rr} = 2S^{(n)}, \qquad (2.8)$$

with source

$$S^{(n)} = -\frac{1}{r}\left[r\left(\frac{g^{(n-1)}}{r}\right)_{,r}\right]_{,r} \qquad (2.9)$$

determined by $g^{(n-1)}$. We keep the same boundary conditions as before, with the proviso $R > 2m$. The perturbation system is seeded by a homogeneous solution $g^{(0)}$ of (2.1). Our primary concern is how the decay of the radiative amplitude is effected by the Schwarzschild mass.

Consider the null parallelogram made up of incoming and outgoing radial characteristics which intersect at vertices P, Q, R, S as depicted in Fig. 1. By integrating Eq. (2.8) over the area Σ bounded by these vertices, we obtain

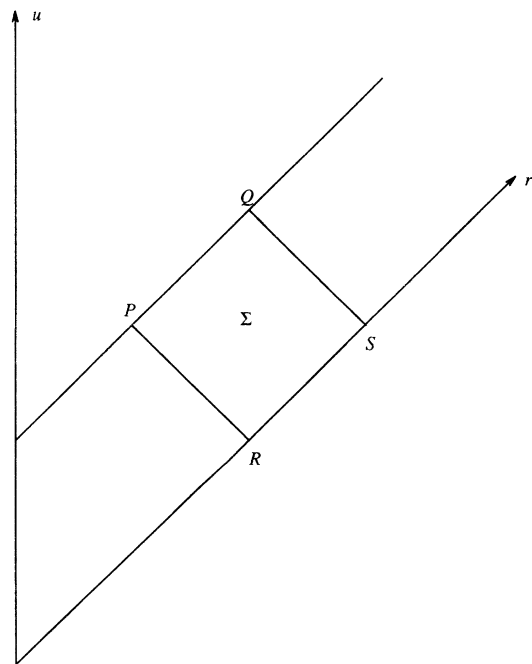$$g^{(n)}_Q = g^{(n)}_P + g^{(n)}_S - g^{(n)}_R + \int_\Sigma S^{(n)}(u', r')du'dr'. \qquad (2.10)$$

FIG. 1. Line segments drawn at $45°$ to the vertical represent radial characteristics. Their intersection defines the fundamental null parallelogram $PQRS$ used in constructing both our analytic and numerical solutions.

This identity may be used to solve the perturbation equations by taking Q to be the field point at (u, r); P to lie on the reflecting barrier, so that $g_P = 0$; and R and S to lie on the initial null cone with coordinates $(0, u/2 + R)$ and $(0, u/2 + r)$, respectively. We seed the expansion with initial data $g^{(0)}(0, r)$, with $g^{(n)}(0, r) = 0$ for $n \geq 1$, so that $g_R^{(n)} = g_S^{(n)} = 0$, for $n \geq 1$. The resulting solution of (2.8), for $n \geq 1$, is

$$g^{(n)}(u, r) = \int_\Sigma S^{(n)}(u', r') du' dr', \qquad (2.11)$$

where the integration region Σ consists of the parallelogram bounded by the outgoing light rays $u' = 0$ and $u' = u$ and by the incoming light rays $u' + 2r' = u + 2R$ and $u' + 2r' = u + 2r$. We will only carry out this scheme to order $n = 1$, at which the corrections to flat space are linear in m.

Consider then a homogeneous wave $g^{(0)}$ whose initial null data have compact support inside a radius R_1, so that $g^{(0)}$ has no tail. Then, for $u > 2(R_1 - R)$, only the outgoing wave in the decomposition (2.2) lies in Σ and there is no contribution to the field from the initial values at points R and S. Consequently, (2.11) gives

$$g^{(1)}(u, r) = \int_\Sigma f(u'/2 + R)/r'^3 du' dr' \qquad (2.12)$$

$$= -8 \int_0^{2(R_1 - R)} f(u'/2 + R) \frac{(r - R)(u - u' + r + R)}{(u - u' + 2r)^2 (u - u' + 2R)^2} du'. \qquad (2.13)$$

This implies that the field observed at fixed r has the late time asymptotic behavior

$$g^{(1)}(u, r) \sim F_0/u^3 \qquad (2.14)$$

and the radiation amplitude has the late time behavior

$$g^{(1)}(u, \infty) = Q^{(1)} \sim F/u^2, \qquad (2.15)$$

where the constants F_0 and F depend upon the details of the initial data. The dependence of (2.14) on proper time or (2.15) on Bondi time is effectively the same.

Thus, to first order in m, a wave with compact initial data in a Schwarzschild background has the same decay behavior as we found for a flat space wave with noncompact initial data Φ_0 having an asymptotic Taylor series expansion with vanishing $1/r^2$ term. This has a simple explanation in terms of backscattering by the curvature of the Schwarzschild background. Although the initial data at $u = 0$ are compact, this backscattering can potentially produce any power of $1/r$ in the null data induced at a later time $u = u_1$, with one exception. It cannot produce a $1/r^2$ term corresponding to the Newman-Penrose constant, which is also conserved by the curved space wave equation. As a result, compact data at $u = 0$ induce data at $u = u_1$, which is generic except that its Newman-Penrose constant vanishes. At times $u \gg u_1$, these data then decay according to the same generic scheme as a flat space wave with vanishing Newman-Penrose constant.

Now consider the decay of waves whose initial data are noncompact. We isolate the same cases as in the flat space analysis. For initial data with $g^{(0)}(0, r) = $ const for $r > R_1$ the decay has the same behavior, (2.14) and (2.15), as for compact initial data. This is because a pure radiation field does not contribute to the source $S^{(1)}$ in the integration region Σ corresponding to late times $u \geq 2(R_1 - R)$. Next consider the noncompact initial data (2.3) for the case $N = 1$, corresponding to a nonzero Newman-Penrose constant. The calculation of $g^{(1)}$ via (2.11) is lengthy but straightforward. The result is given

in the Appendix. At a fixed, finite value of r, this leads to the asymptotic behavior

$$g^{(1)}(u, r) \sim \frac{4R(R - r)}{ru^2} + O\left(\frac{1}{u^3}\right) \qquad (2.16)$$

and, at null infinity,

$$Q^{(1)}(u, r) \sim \frac{4R \ln u}{u^2} + O\left(\frac{1}{u^2}\right). \qquad (2.17)$$

According to (2.16), the decay at fixed r has the same $1/u^2$ behavior as the corresponding decay of the zeroth order flat space wave $g^{(0)}$. However, according to (2.17), the first order radiation amplitude $Q^{(1)}$ decays faster than the $1/u$ decay of $Q^{(0)}$. Thus, to this order, the decay of the radiation field is not affected by backscattering and has the same time dependence as a flat space wave with nonzero Newman-Penrose constant.

For noncompact data (2.3) with $N > 1$, first note that

$$g_N^{(0)} = \frac{1}{(N - 1)!}(-2R\partial_u)^{N-1} g_1^{(0)}. \qquad (2.18)$$

As a result, since the perturbation equation (2.7) is invariant with respect to the time translation operator ∂_u, the perturbation satisfies

$$\Box^{(2)} \left[g_N^{(1)} - \frac{1}{(N - 1)!}(-2R\partial_u)^{N-1} g_1^{(1)} \right] = 0. \qquad (2.19)$$

This implies that $g_N^{(1)}$ satisfies the equivalent of (2.18), up to a homogeneous solution H of the flat space wave equation,

$$g_N^{(1)} = \frac{1}{(N - 1)!}(-2R\partial_u)^{N-1} g_1^{(1)} + H. \qquad (2.20)$$

Since $g_N^{(1)}(0, r) = 0$ by assumption, the homogeneous solution is determined by the initial value of $\partial_u^{N-1} g_1^{(1)}$. Because of the Newman-Penrose conservation law, a $1/r$ expansion of $\partial_u^{N-1} g_1^{(1)}(0, r)$ has no $1/r$ term, but other-

wise the expansion is generic. According to our results for the decay of flat space waves, this implies that $H(u,r) = O(1/u^3)$ and $H(u,\infty) = O(1/u^2)$. On the other hand, $\partial_u^{N-1} g_1^{(1)}$ decays as $O(1/u^{N+1})$ and $\partial_u^{N-1} Q_1^{(1)}$ decays as $O(\ln u/u^{N+1})$, because the order relations (2.16) and (2.17) obtained from the solution for $g_1^{(1)}(u,r)$ (given in the Appendix) are differentiable with respect to u. Putting these results together, we infer the leading order time dependence $g_N^{(1)} = O(1/u^3)$ and $Q_N^{(1)} = O(1/u^2)$, for $N > 1$.

III. SELF-GRAVITATING WAVES

Given initial data which is smooth at null infinity, i.e. has an asymptotic $1/r$ expansion, the leading order perturbation results of Sec. II for the late time decay can be summarized as follows. Let $P = -r^2 \partial_r r \Phi|_{r=\infty}$ be the Newman-Penrose constant. Then, if $P \neq 0$,

$$g^{(0)}(u,r) + mg^{(1)}(u,r) \sim \frac{4P(R-r)}{u^2}\left(1 + \frac{m}{r}\right) + O(1/u^3)$$

$$(3.1)$$

and

$$Q^{(0)}(u,r) + mQ^{(1)}(u,r) \sim -\frac{2P}{u} + \frac{4mP\ln u}{u^2} + O(1/u^2).$$

$$(3.2)$$

Otherwise, if $P = 0$, $g^{(0)}(u,r) + mg^{(1)}(u,r) = O(1/u^3)$ and $Q^{(0)}(u,r) + mQ^{(1)}(u,r) = O(1/u^2)$. In the latter case, the backscattering to linear order in m produces tails which lead to the same generic decay for both compact and noncompact initial data. Accordingly, there are two distinct types of late time decay determined by whether or not the Newman-Penrose constant vanishes.

We now use solutions obtained by numerical evolution to check the validity of these "linear in m" results in the full test field case and to examine their extension to strongly self-gravitating waves. In all the numerical simulations, we have set the location of the reflecting boundary at $R = 1$.

A. Compact initial data

As an example of initial data of compact support we choose the incoming pulse

$$g(u_0,r) = \begin{cases} \lambda[4(r-1)(r-2)]^6 & \text{for } 1 \leq r \leq 2 \\ 0 & \text{for } r \geq 2, \end{cases} \quad (3.3)$$

which is normalized to have maximum value λ.

We first consider the perturbative regime by setting $\lambda = 10^{-4}$ and $m = 0.2$, so that the wave has negligible nonlinearity but the interior mass produces the redshift $dt/d\tau \approx 1.3$ between the reflector and infinity, which represents the full perturbative as opposed to the "linear in m" regime. Figure 2 displays the corresponding graph
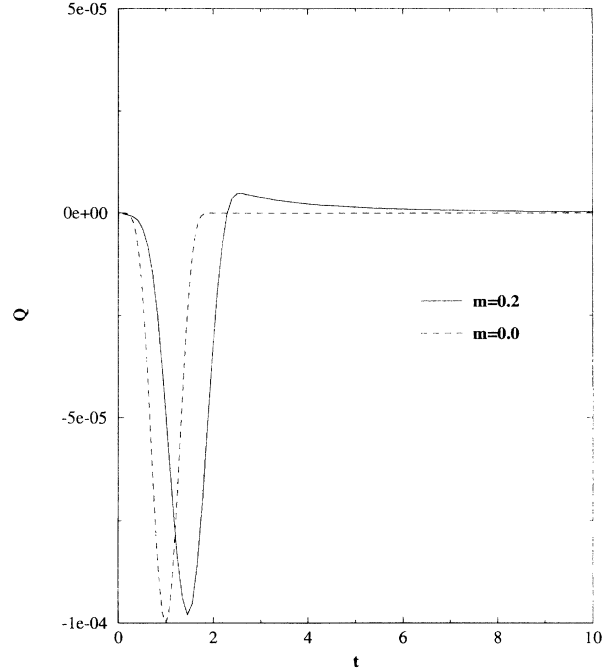
FIG. 2. Radiation amplitude $Q(t)$ vs Bondi time t, compared to the radiation profile for a flat background $m = 0$.

of the radiation amplitude $Q(t)$ vs Bondi time t, superimposed for purposes of reference on the corresponding tail-free solution in a flat background, obtained by setting $m = 0$. In addition to redshifting the radiation amplitude, the interior mass introduces one extra oscillation before the final decay. The late time power law decay of the radiation tail of this solution is best illustrated by a graph of $t^2 Q$ vs Bondi time, which is shown in Fig. 3.
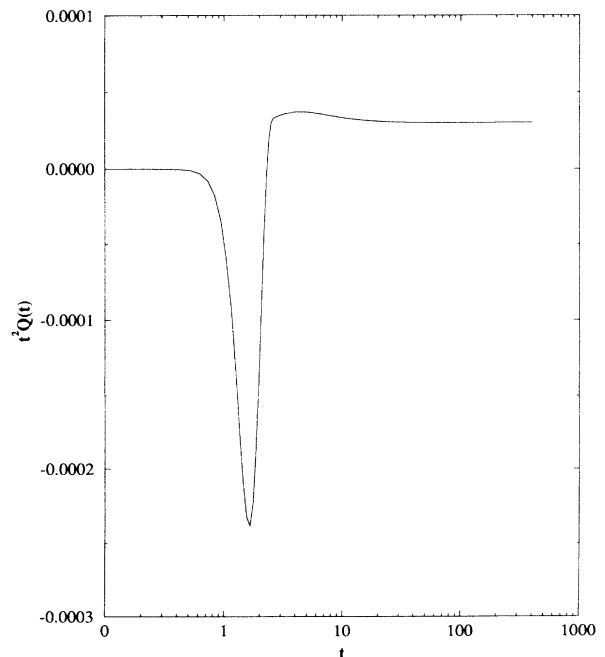
FIG. 3. The graph of $t^2 Q$ makes evident the power law decay of the radiation for the compact data (3.3).

The constancy of this graph at large Bondi times confirms the $1/t^2$ decay found for the "linear in m" solution. A fit of $\ln(Q)$ vs $\ln(t)$ to a straight line in the interval from $t = 10$ to $t = 400$ gives a power law coefficient 2.006, in excellent agreement with the value 2. Similarly, the late time decay of the field computed at finite r also exhibits the $1/t^3$ behavior found analytically in the "linear in m" regime. The computed power law coefficient is 2.936.

For purposes of exhibiting the tail in the strongly non-linear regime, we next consider the pulselike data (3.3) with $\lambda = 0.4$. In this regime, we set $m = 0$ since the background mass plays no essential role because this field is well beyond the critical amplitude to collapse to a black hole on its own. Only a small fraction of the initial energy is radiated to infinity and an horizon with final Bondi mass $M_H \approx 0.86$ forms in the exceedingly short proper time $\tau \approx 0.0004$, measured along the reflector's world line. The graph of $t^2 Q(t)$ vs Bondi time in Fig. 4 clearly exhibits a $1/t^2$ decay of the radiation tail of this highly nonlinear solution. However, this power law decay becomes the predominant signal only after the Bondi time $t = 200$, at which the redshift has reached the enormous value of 6×10^{10}.

B. Noncompact initial data

Now consider the initial data

$$g(0, r) = \lambda(1 - 1/r), \tag{3.4}$$

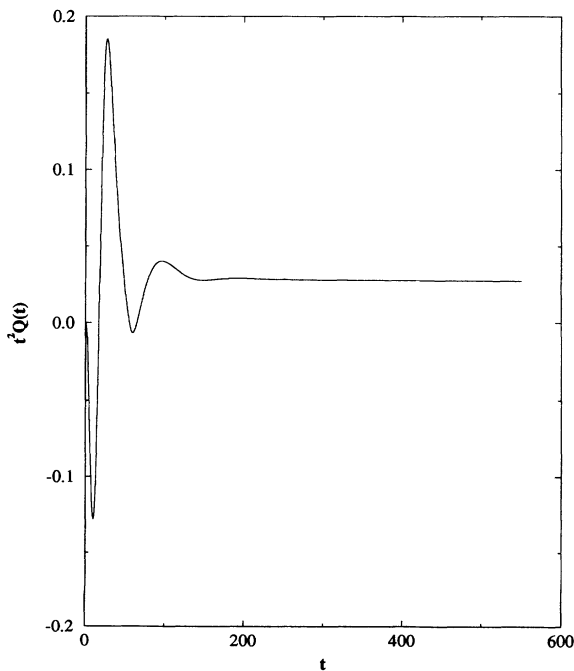corresponding to the $N = 1$ data (2.3) with nonvanishing Newman-Penrose constant $P = -\lambda$. In order to
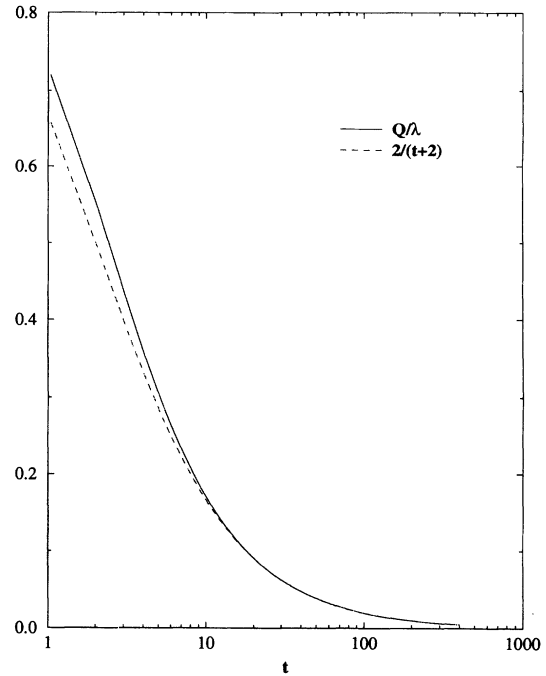
FIG. 5. The final decay of the radiation amplitude from (3.4) with $\lambda = 10^{-4}$ and $m = 0.2$ has the asymptotic form $Q(t) \sim 2\lambda/(t + 2)$ of the flat space solution.

treat the perturbative regime, we again set $\lambda = 10^{-4}$ and $m = 0.2$. Figure 5 shows how the final decay of the radiation amplitude approaches the asymptotic form $Q(t) \sim 2\lambda/(t + 2)$ of the flat space solution. Figure 6 shows how the numerical solution manifests the asymptotic relation $tQ \sim -2P = 2\lambda$ predicted by (3.2). The
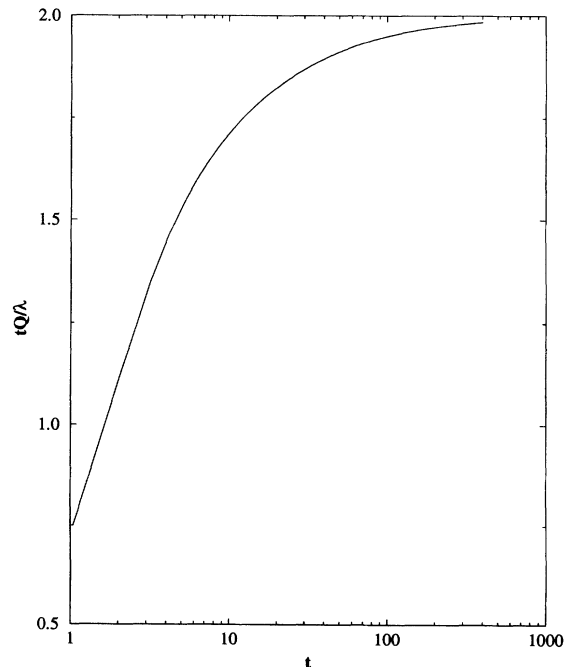
FIG. 4. For $\lambda = 0.4$ and $m = 0$ in (3.3), the graph of $t^2 Q(t)$ vs Bondi time exhibits a $1/t^2$ decay, which becomes the predominant signal only after the Bondi time $t = 200$, at which the redshift has reached the enormous value of 6×10^{10}.

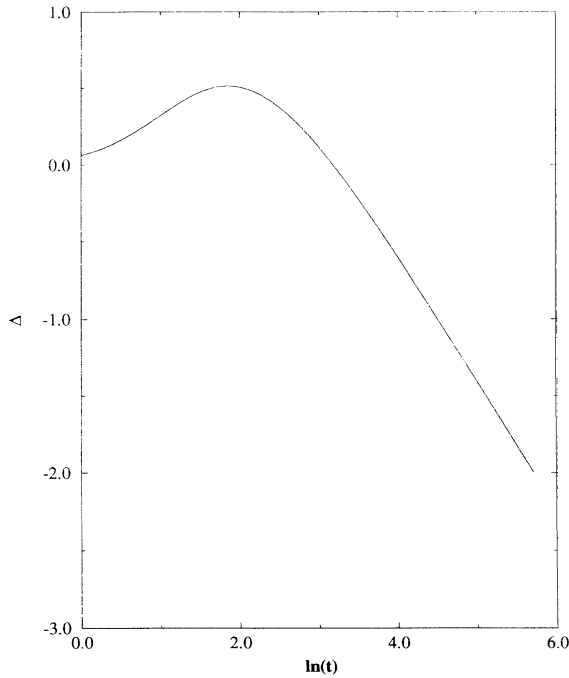FIG. 6. The numerical solution manifests the asymptotic relation $tQ \sim -2P = 2\lambda$ predicted by (3.2).

FIG. 7. In the "linear in m" regime, $\Delta \sim 4mP\ln(t)/\lambda + O(1)$, according to (3.2).
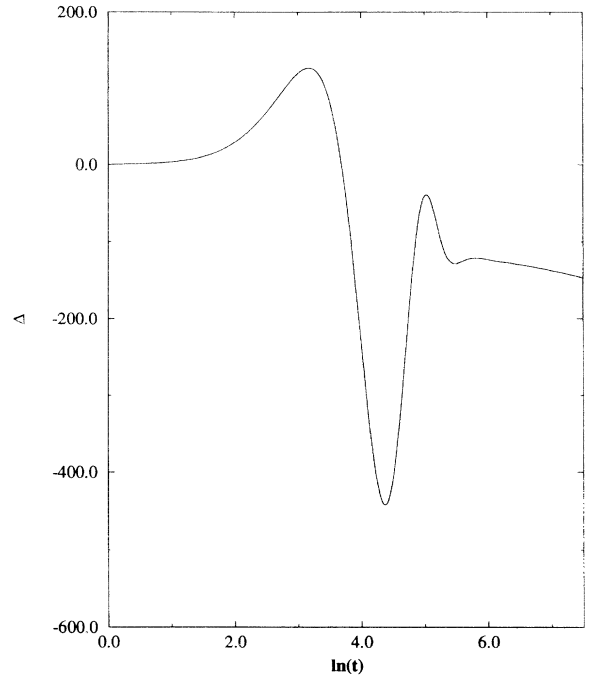

FIG. 9. The graph of Δ shows the logarithmic correction to the decay in the nonlinear regime.

curvature dependent logarithmic term in (3.2) can also be extracted by subtracting out the flat space solution. We define

$$\Delta = t^2[Q/\lambda - 2/(t+2)], \qquad (3.5)$$

so that in the "linear in m" regime $\Delta \sim 4mP\ln(t)/\lambda + \text{const}$, according to (3.2). This is plotted vs $\ln(t)$ in Fig. 7. At late time, the graph has slope -0.83, in agreement with the "linear in m" prediction $4mP/\lambda = -0.8$ to well within the 20% accuracy expected from $O(m^2)$ corrections. Similarly, at fixed r the field decays in accord with (3.1).
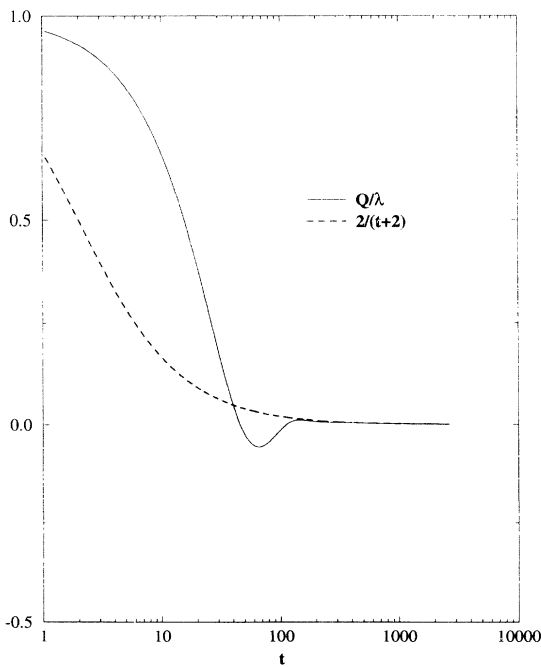

FIG. 8. In the nonlinear regime, the numerical solution again has the asymptotic form $Q(t) \sim 2\lambda/(t+2)$ of the flat space solution.
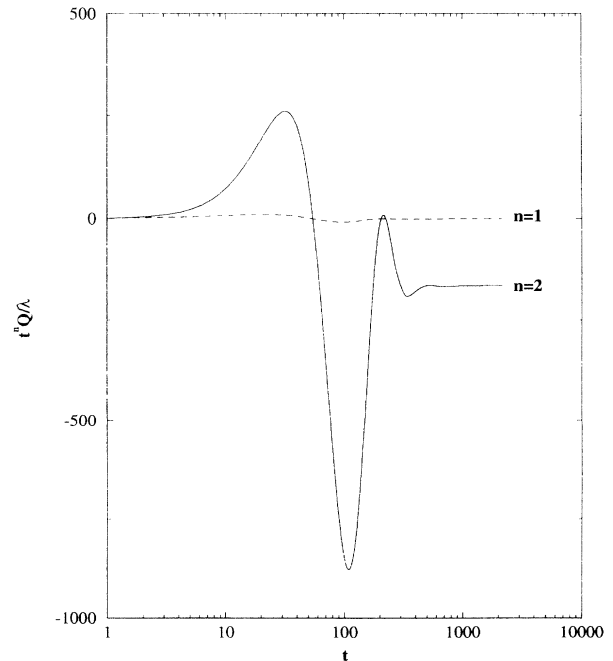

FIG. 10. Graphs of the radiation field, for the data (3.6) in the highly nonlinear case $\lambda = 3$, clearly indicate a $1/t^2$ decay.

In order to study the evolution of the data (3.4) in the strongly nonlinear regime, we set $\lambda = 3$ and $m = 0$. This system has initial Bondi mass $M_0 \approx 5.8$ and forms a black hole with final Bondi mass $M_H \approx 2.87$ in proper time $\tau \approx 9.6 \times 10^{-8}$, measured along the reflector's world line. Figure 8 shows how the decay approaches the flat space behavior characteristic of a nonvanishing Newman-Penrose constant. In Fig. 9, we extract the flat space term to show how the logarithmic correction carries over to the nonlinear regime. At late time, the graph of Δ has an approximate slope of -20, corresponding to $4mP/\lambda$ for the value $m = 5$ lying between M_0 and M_H.

Finally, consider the initial data

$$g(0, r) = \lambda(1 - 1/r^2), \qquad (3.6)$$

which have a nonvanishing initial monopole moment but a zero Newman-Penrose constant. Figure 10 shows graphs of tQ and t^2Q for the radiation field in the highly nonlinear case $\lambda = 3$. The initial mass is $M_0 \approx 6.5$ and the system forms a black hole with mass $M_H \approx 4.2$ in the reflector's proper time $\tau \approx 5.5 \times 10^{-23}$. The graphs clearly indicate a $1/t^2$ decay, in agreement with the prediction of the "linear in m" approximation. This establishes, in the nonlinear regime, that a nonzero initial monopole moment does not produce an $O(1/t)$ decay, in contrast with a nonzero initial Newman-Penrose constant.

IV. CONCLUSION

The analytic and numerical results for our model are in essential agreement with the work of Gundlach, Price, and Pullin [5,6]. This confirms that their conclusions regarding power law tails are generic and not sensitive to choice of boundary conditions or numerical algorithm. In both the perturbative and nonlinear regimes we find in addition that the Newman-Penrose constant determines the order of the power law decay. For the radiation field, the amplitude decays as $1/t$ for the case of a nonvanishing Newman-Penrose constant, and otherwise, as $1/t^2$ in the generic case. This clarifies the previous hypothesis [1,6] that the choice between these two power laws rested upon whether the system had a nonvanishing initial scalar monopole moment. In that work, the exact static monopole solution, which was used to model an initial monopole, also has nonvanishing Newman-Penrose constant, so that the individual effects of monopole moment and Newman-Penrose constant were not isolated. (This is a quirk of the curved space solution since the flat space $1/r$ static monopole has vanishing Newman-Penrose constant.) However, our results clearly show

that initial data with nonzero monopole moment but zero Newman-Penrose constant have a radiative $1/t^2$ power law decay. It is the conserved Newman-Penrose quantity that plays the deciding role.

In the pure self-gravitating case, for which the background mass m of the interior vanishes, the power law decay only becomes apparent at enormous redshifts for which there is potential of numerical underflow to affect the accuracy of the numerical results. By being overly conservative and stopping the evolution before this possibility, previous work [4] led to the erroneous conclusion that the final radiative decay was exponential, with respect to Bondi time. It is now clear that this was the result of stopping the evolution prematurely in the quasi-normally damped stage. An inspection of our numerical algorithm shows that underflow is a serious problem in the interior region where the time step is very small but this is countered by the large redshift in the exterior to give reliable results for the radiation field. Caution is still warranted in extending numerical results to time infinity, where a true singularity in the conformal geometry exists. Nevertheless, there is a time scale at which the transition from exponential to power law decay is cleanly discernible and consistent with the expectations of perturbation theory. Furthermore, within the time interval explored, the numerical results in the nonlinear regime confirm the logarithmic corrections to the tail corresponding to the analytic approximation (2.17).

APPENDIX

We give here the expression for $g^{(1)}$ for the noncompact initial data (2.3), with $N = 1$. For simplicity we have set $R = 1$.

$$g^{(1)}(u, r) = -\frac{N_1}{D_1} - \frac{N_2}{D_2} + \frac{N_3}{D_3} - \frac{N_4}{D_4},$$

where

$$N_1 = 4\,(u^4 + 20\,u^3 + 32\,r\,u^2 + 108\,u^2 + 32\,r^2\,u + 160\,r\,u + 224\,u + 96\,r^2 + 192\,r + 160)\,\ln(1 + u/2),$$

$$N_2 = 4\,(r - 1)\,(u^5 + 10\,r\,u^4 + 8\,u^4 + 26\,r^2\,u^3 + 50\,r\,u^3 + 20\,u^3 + 20\,r^3\,u^2 + 104\,r^2\,u^2 + 84\,r\,u^2 + 16\,u^2$$
$$+ 64\,r^3\,u + 144\,r^2\,u + 48\,r\,u + 64\,r^3 + 64\,r^2),$$

$$N_3 = 4(u^2 + 4\,r\,u + 8\,u + 4\,r^2 + 16\,r + 8)\,\ln[1 + u/(2\,r)],$$

$$N_4 = 4\,\ln[(u + 2\,r)/r\,(u + 2)],$$

$$D_1 = (u + 2)^2 (u + 4)^2 (u + 2\,r + 2)^2,$$
$$D_2 = r\,u\,(u + 2)^2 (u + 4)\,(u + 2\,r)^2 (u + 2\,r + 2),$$
$$D_3 = (u + 2\,r)^2 (u + 2\,r + 2)^2,$$
$$D_4 = u^2.$$

[1] R. H. Price, Phys. Rev. D **5**, 2419 (1972).

[2] B. G. Schmidt, in Proceedings of the 4th Hungarian Relativity Workshop, edited by S. Perjes (unpublished).

[3] H.-P. Nollert and B. G. Schmidt, Phys. Rev. D **45**, 2617 (1992).

[4] R. Gómez and J. Winicour, J. Math. Phys. **33**, 1445 (1992).

[5] C. Gundlach, R. Price, and J. Pullin, Phys. Rev. D **49**, 883 (1994).

[6] C. Gundlach, R. Price, and J. Pullin, Phys. Rev. D **49**, 890 (1994).

[7] D. Christodoulou, Commun. Math. Phys. **105**, 337 (1986).

[8] R. Gómez, R. Isaacson, and J. Winicour, J. Comput. Phys. **98**, 11 (1992).

[9] D. Christodoulou, Commun. Math. Phys. **109**, 613 (1987).

[10] M. W. Choptuik, in *Approaches to Numerical Relativity*, edited by R. d'Inverno (Cambridge University Press, Cambridge, England, 1992), p. 202.

[11] M. W. Choptuik, Phys. Rev. Lett. **5**, 9 (1993).

[12] E. T. Newman and R. Penrose, Proc. R. Soc. London **A305**, 175 (1968).